FACHHOCHSCHULE AACHEN (FH)
Campus Jülich
UNIVERSITY OF APPLIED SCIENCES

Fachbereich: Energietechnik
Studiengang: Physikingenieurwesen

FH AACHEN
UNIVERSITY OF APPLIED SCIENCES

Structuring and Depth Profiling with an Argon Ion Gun

Bachelorarbeit

von

Zheng, Ying

October, 2014

angerfertigt am
Jülich Centre for Neutron Science, JCNS-2,
und Peter Grünberg Institut, PGI-4:
Streumethoden
Forschungszentrum Jülich GmbH

Jülich Centre for Neutron Science

JÜLICH
FORSCHUNGSZENTRUM

Diese Arbeit wurde betreut von:

Herrn Prof. Dr. Arnold Förster

Herrn Dr. Alexander Weber

Diese Arbeit ist von mir selbstständig angefertigt und verfasst worden. Es sind keine anderen als die angegebenen Quellen und Hilfsmittel verwendet worden.

Jülich 30.09.2014 — Zheng, Ying

Ort, Datum — Zheng, Ying

Contents

1 Introduction **1**

2 Introduction to sputtering **3**

3 Experimental Methods **4**

3.1 Principles of Sputter Gun 4

3.1.1 Gas Ionization 5

3.1.2 Ion Extraction 6

3.1.3 Wien Mass Filter 7

3.1.4 Ion Focusing and Deflection 9

3.1.5 Current Measurement 10

3.2 MBE 11

3.3 Auger Electron Spectroscopy (AES) 13

3.4 X-ray reflectometry 16

4 Preliminary Works **19**

4.1 Preparations of Sputter Gun 20

4.2 Start of Operation 21
4.3 Optimization of Beam Size 24
4.4 Sputter Position 28

5 Results and Discussion **34**
5.1 Measurement 1 34
5.2 Measurement 2 36
5.3 Measurement 3 41

6 Conclusion and Outlook **45**
6.1 Conclusion 45
6.2 Outlook 46

Bibliography **49**

Chapter 1

Introduction

The function of a sputter gun is removing atoms on a solid target material. It is widely applied in thin film techniques, such as cleaning a substrate surface, structuring a thin film and doing a depth profiling in combination with Auger Electron Spectroscopy (AES). With a sputter gun, contaminations on the sample surface can be removed. Since it can sputter off the material on the sample surface, it can structure thin films in the expected way. The structuring thin films plays an important role in creation of devices in the semiconductor industry. Depth profiling is an important analytical technique for thin films. The basic procedure of depth profiling is recording the element specific peaks during the sputtering. With AES, the composition of a target material can be determined. The result will show the concentration of a sample as a function of the sputter time. For a constant ion energy and beam current, the rate should be constant, so the sputter time is proportional to the sputtered depth.

Since the sputter gun is newly equipped, the first step is operating the sputter gun correctly. Set correct parameters to get a fine focused ion beam. The sputter position and sample orientation need to be determined. Calculation of the

sputter rate for different materials is a perquisite for both structuring thin films and depth profiling. To determine the sputter rate, a thin layer is deposited on the substrate and is sputtered step by step and analysed using the AES after each sputtering step. The thickness change can be determined by the AES spectrum. Here Fe and Au are deposited on a silicon substrates to determine the sputter rate. From the result, we find that there is no linear dependency between sputtered depth and sputter time. This phenomenon will be discussed in this thesis.

Chapter 2

Introduction to sputtering

With a sputter gun, an ion beam can be generated. When the incident ion reaches the target surface, it will lose its energy due to collisions and transfer energy and momentum to the surface atoms [1]. If the surface atoms get enough energy, they will be displaced from their initial positions. These displaced atoms, in turn, displace other substrate atoms and result in collision cascades. If the displaced atoms reach the surface and get enough energy to overcome the surface binding energy, they will be ejected from the surface, which is called sputtering[2].

Chapter 3

Experimental Methods

In this chapter, the way of how a sputter gun works is explained in detail. Since samples need to be deposited by thin film techniques, the Molecular Beam Epitaxy (MBE) is introduced as well. For the sample analysis, AES and X-ray reflectometry (XRR) are applied. There will be also some brief introductions for these two methods.

3.1 Principles of Sputter Gun

The sputter gun consists of an ion source power supply QIE12/38 and a Wien mass filter (see Figure 3.1). It can be used to clean a sample surface, to structure thin films and to do depth profilings together with AES. The sputtered shape can be rectangles, lines or dots and a selected area can be homogeneously sputtered. The size of the beam is adjustable. There are two operation modes, fine focused mode (small focus) and high current mode (large focus). In the high current mode, more material can be removed. All inert gases can be used as the operating gas [3]. Here argon gas is used to generate the ion beam. The beam energy

can be changed in the range of 0 eV up to 5 keV and typical beam currents are in range of 1 pA up to 10 μA [3]. A Wien mass filter is used to purify the beam. Only the defined ions can pass the filter. The double charged ions or neutrals will be filtered.

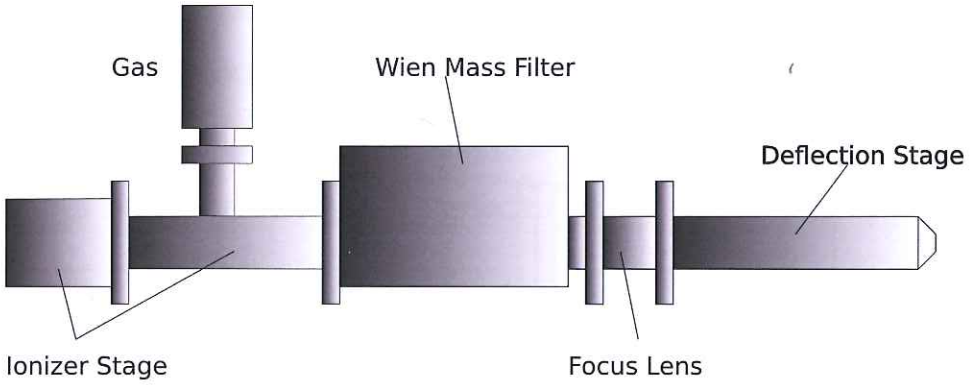

Figure 3.1 – Schematic of Sputter gun - ion source IQE 12/38 and Wien mass filter

3.1.1 Gas Ionization

Figure 3.2 shows the ionization assembly of the sputter gun. A cylindrical anode cage and a filament are mounted in a cylindrical repeller. The Ω - shaped iridium ribbon filament is mounted around the anode cage in a distance of 7 mm [3]. The filament is heated up by a source power supply. When the electron near the surface of filament gets enough thermal energy, it can overcome the attraction from the metal atoms and leave the metal surface [3]. The emitted electrons are accelerated to the anode cage and collide with the gas, which is introduced via a gas feed - through. If the impact has sufficient energy, an electron can be removed from a gas molecule or atom, forming a positive ion. Thus, the gas is ionized and forms an electron - ion plasma. If an electron has not collided with a gas molecule, it will leave the anode cage and be accelerated by a repeller back to the anode [3]. This process will be repeated until the electron collides with a

gas molecule. In this way the collision efficiency is improved. The number of produced ions depend on the number of electrons emitted, their energy, the type of gas and the number of gas molecules present to be ionized [4].

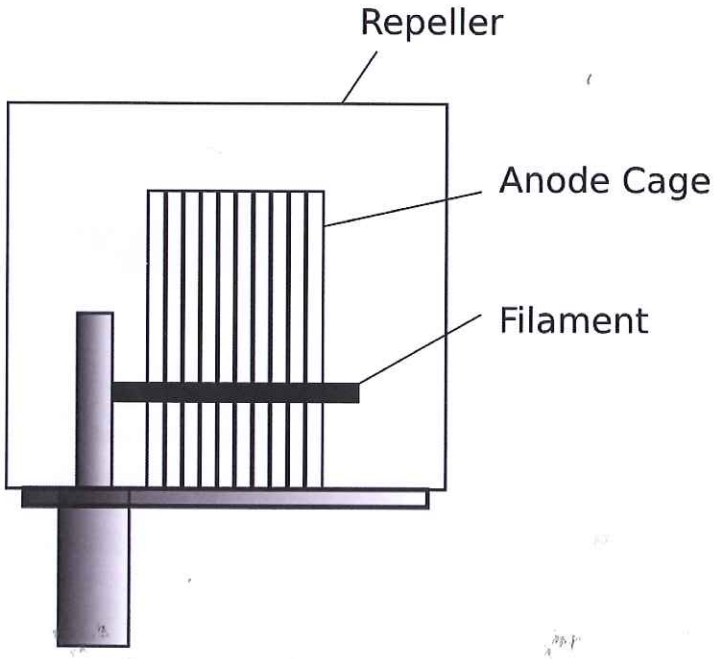

Figure 3.2 – Ionization takes place in this assembly

3.1.2 Ion Extraction

Ions are accelerated out of the plasma by an extractor electrode, which is internally connected to the repeller [3]. A single electrostatic lens works as an extractor. It only can pass the ions, which move close to the system axis. The extractor voltage can be monitored by the source power supply and is displayed in % of beam energy.

3.1.3 Wien Mass Filter

For accurate depth profiling analysis, the ion beam should be of high purity. As shown in Figure 3.1, the Wien Mass Filter is mounted following the ionizer stages. It only allows defined ions to pass and suppresses double charged ions and neutrals by the combination of an electric (E) and a magnetic (B) fields [5]. The Wien Mass Filter consists of a permanent magnet (magnetic field density B) and a pair of electrostatic deflector plates (electric field E), arranged perpendicular to each other.

The ionized particles are accelerated to the velocity v by a constant electric potential U_B [5]. Since the velocity v is not comparable to the velocity of light, the kinetic energy can be shown as:

$$E_{kin} = qU_B, \tag{3.1}$$

$$E_{kin} = \frac{1}{2}mv^2. \tag{3.2}$$

Combination of Equation 3.1 and Equation 3.4 leads to:

$$\frac{1}{2}mv^2 = qU_B, \tag{3.3}$$

with

m	mass of charged particle,
v	velocity of charged particle,
q	charge of particle,
U_B	accelerating voltage of ions.

Equation 3.1 can be transformed to:

$$v = \sqrt{\left(\frac{2eU_B}{m}\right)}. \tag{3.4}$$

Equation 3.4 shows the relationship between the velocity and mass. Particles with different masses will get different velocities. When the particles go into mass filter, they will get two kinds of forces: the electric force and the Lorentz force. These two forces are opposite in directions.

$$|F_{el}| = |F_l|,$$

$$qE = qvB, \tag{3.5}$$

$$v = \frac{E}{B}, \tag{3.6}$$

with

F_{el}	electric force,
F_l	Lorentz force,
E	electric field,
B	magnetic field density.

The particles with velocity $v = \frac{E}{B}$ can pass through the mass filter without changing their trajectories. It means, only the defined particles can pass through the mass filter. In this way, the purity level of the beam is improved. There is a split cylindrical lens "STIGMATOR" in front of the exit aperture. It is used to align the beam to enter the focus section. The beam can be adjusted in the non - dispersive direction (x - direction of the sputter gun) by applying different

potentials to the electrodes of the lens. The working principle is same with the deflection plates. In the dispersive direction (y - direction of sputter gun), the beam is adjusted by the electric field in the mass filter using the "MASS" dial [5].

3.1.4 Ion Focusing and Deflection

In addition to the extractor, a dual lens system is used to focus the ion beam. There are two pairs of plates x_1, x_2 and y_1, y_2 (as shown in Figure 3.3) following the focusing lenses to control the path of the beam [3]. Voltages are applied to these two pairs of plates by the source power supply and two electrostatic fields are produced. These electrostatic field can bend the beam in orthogonal directions. In this way, the beam can be controlled to move around on the sample.

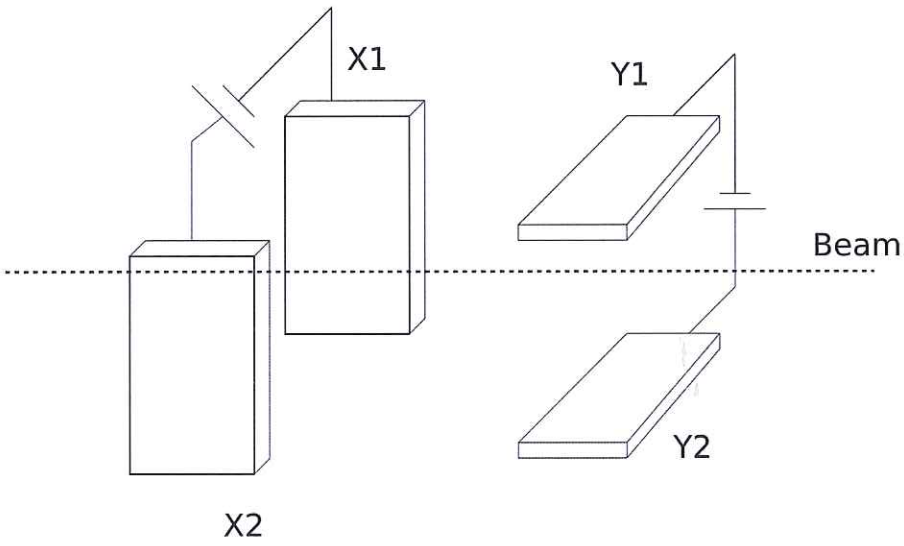

Figure 3.3 – Voltages are applied to two pairs of deflection plates, so that the beam can be controlled to move around.

3.1.5 Current Measurement

Because an ion beam is invisible to the eye, it must be observed by some kind of detector. A Faraday cup is appropriate to detect and measure the beam current. Here we use the manipulator as a Faraday cup. The part holding the sample is connected with a wire to an electrical feed - through, which is connected to ground through an ammeter and a voltage source. Behind the sample, there is a heater, which is also grounded. Figure 3.4 shows a circuit for current measurement using the manipulator. It is possible to determine the beam size using a sample with a pinhole, which is slightly larger than the beam size. The detail of determination of the beam size is explained in Section 4.3.

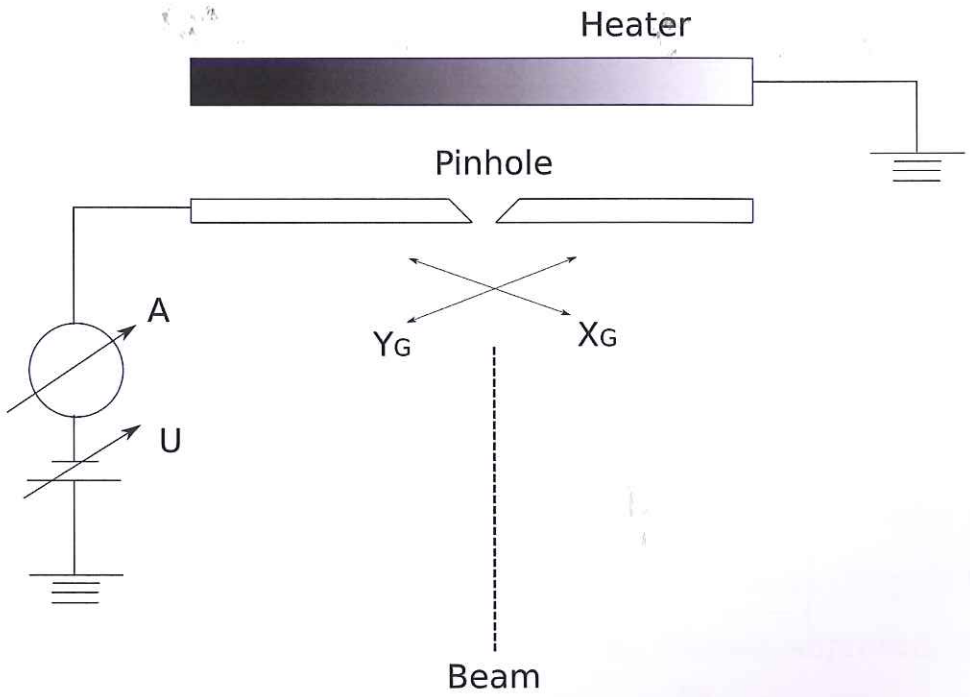

Figure 3.4 – The manipulator is used as a Faraday cup. This figure shows the circuit for beam current measurement.

3.2 MBE

In order to study the working quality of the sputter gun, growing layers on a substrate is the first thing to do. Here the Molecular Beam Epitaxy (MBE) is applied to grow thin films. MBE is a thin film deposition technique with low deposition rates. Molecules of a material are deposited on a substrate and form a thin layer. The crystal surface of the substrate dictates the arrangement of the adsorbed atoms, so the lattice spacing of the substrate and grown crystal should be close to each other [6]. Figure 3.5 shows the MBE system. It consists of several vacuum chambers.

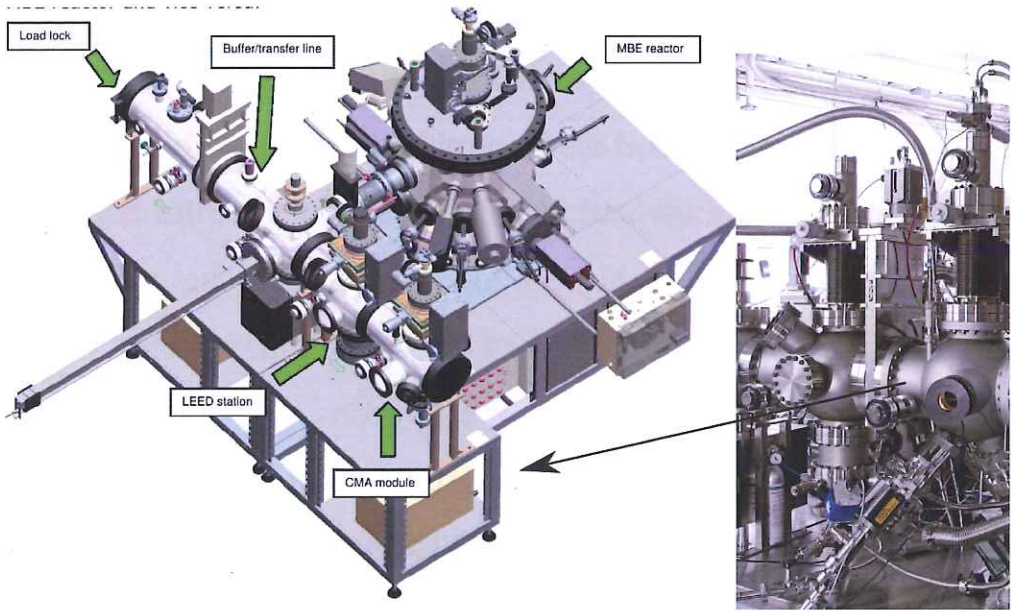

Figure 3.5 – This is a overview of MBE system. The right side picture shows the analysis chamber, which is mounted at the end of bufferline as shown in figure [7]

A load - lock is used for entry and exit of samples without influencing the pressure in the main chamber. The load - lock is equipped with a turbo pump and a scroll pump and the pressure can reach to 10^{-8} mbar range.

A buffer line is for transferring samples and is equipped with Low - energy electron diffractometer (LEED). It is pumped by an ion pump and the pressure in bufferline is around 10^{-11} mbar.

An analysis chamber, which includes a sputter gun and AES, is mounted at the end of the buffer line. The chamber is pumped by a turbo pump and a scroll pump and the pressure in the chamber is around 10^{-10} mbar.

The main chamber is mounted with all solid sources for thin film growth and a Reflection high - energy electron diffractometer (RHEED) to analyse the crystal structure of the surface. Vacuum is the prerequisite for the thin film growth. The UHV condition avoids that the molecules in the environment contaminate the beam and the surface of the substrate. A Liquid Nitrogen cryopanel is mounted surrounding the samples. They can provide large pumping speeds for residual gases, notably H_2O and also CO_2 [8]. A combination of a scroll pump for the rough to medium vacuum range and a turbo pump for the ultra high vacuum range is connected in series to achieve a low pressure. In the main chamber, there is also a 10k cryopump with a closed - cycle helium system. With these pumps the pressure can reach as low as 1×10^{-11} torr.

The molecular beam is produced by heating up a solid source. Here sources are evaporated by using effusion cells and electron beams. The evaporated molecules impinge on a substrate surface and form a thin film. The effusion cell consists of a crucible, a tantalum filament (surrounding heat shield) and a thermocouple [9]. The source is heated by a heat shield and forms a reasonably stable flux. With an effusion cell, the deposition rate is easily controlled by changing the temperature of source, but it can not withstand extremely high temperature (above 1800°C). In this case, heating the source directly with a high

energy beam is much better than using an effusion cell. The source is put in a water - cooled crucible and an intense electron beam is directly impinging on the material [10]. By using an electron beam, a material with extremely high evaporate points can be used, but the deposition rates of some materials are hard to be stabilized.

To monitor the deposition rate, Quartz Micro Balances (QMB) are mounted in the main chamber. QMB is an instrument, which can measure small mass changes. The basic principle of QMB is, that its resonant frequency depends on the mass of crystal [6]. Equation 3.7 shows the relationship between mass change and frequency change. Here m is the mass of crystal and ν is the resonance frequency. The Δ describes the change. The resonance frequency decreases, when the mass of the crystal increases due to deposition [6]. The frequency and rate changes can be monitored. Since QMB are mounted at sample position, the deposition rate can be monitored during deposition.

$$\frac{\Delta m}{m} \propto -\frac{\Delta \nu}{\nu} \tag{3.7}$$

3.3 Auger Electron Spectroscopy (AES)

AES is an analytical technique, which plays an important role in the depth profiling. It can be used to identify elements on the sample surface. With the intensity information provided by a AES spectrum, a quantitative determination of the layer thickness is also possible. AES uses a focused beam of primary electrons to probe the sample surface. As a consequence of interaction, the inner shell electron is kicked out. Now it is not a ground state, so the vacancy is

filled by an outer shell electron. Since the electron moves to the lower energy level, it will lose an amount of energy, which is equal to the difference energy of orbitals [11]. This energy is transferred to another outer shell electron and this electron is emitted. The emitted electron is the so called Auger electron. The energies of Auger electrons are characteristic for different elements. They can be detected when the electrons are emitted without inelastic scattering in solid. The interaction is shown in Figure 3.6. These emitted Auger electrons are collected by the analyser. The amount of Auger electrons can be plotted as a function of kinetic energy of the Auger electrons. The spectrum is normally shown in derivative mode, as shown in Figure 3.7. In the direct spectrum, the Auger electron peaks are small and hard to be recognized due to the large background. When it is represented in derivative mode, the peaks get bigger and are easier to be observed.

Since electrons have a short mean free path in solids, Auger electrons can only escape from the outer $0.4 \sim 5$ nm of a solid at their characteristic energy, so AES is highly surface sensitive [12]. When AES is combined with a sputter gun, it can do the depth profiling and the result can be shown as element intensities versus sputtering time, or layer thickness versus sputtering time.

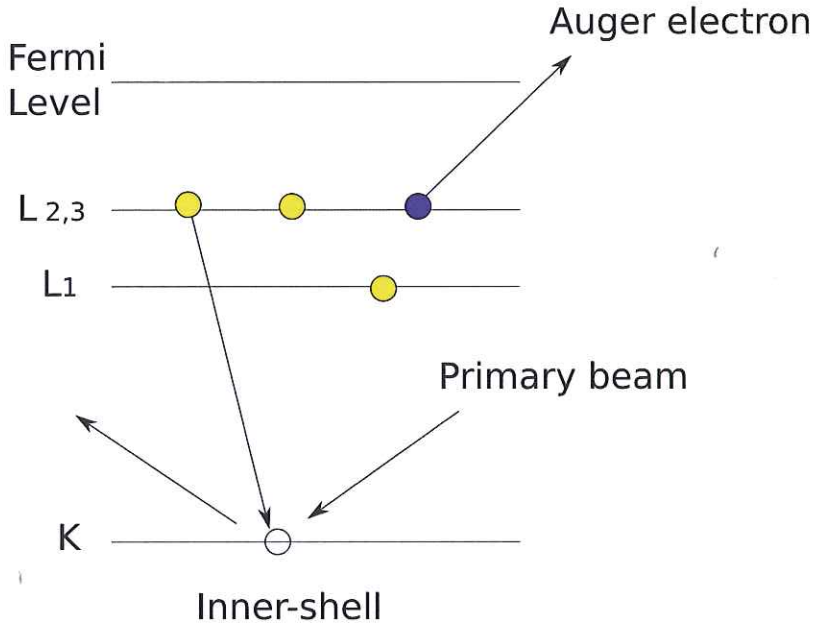

Figure 3.6 – Schematic representation of Auger effect

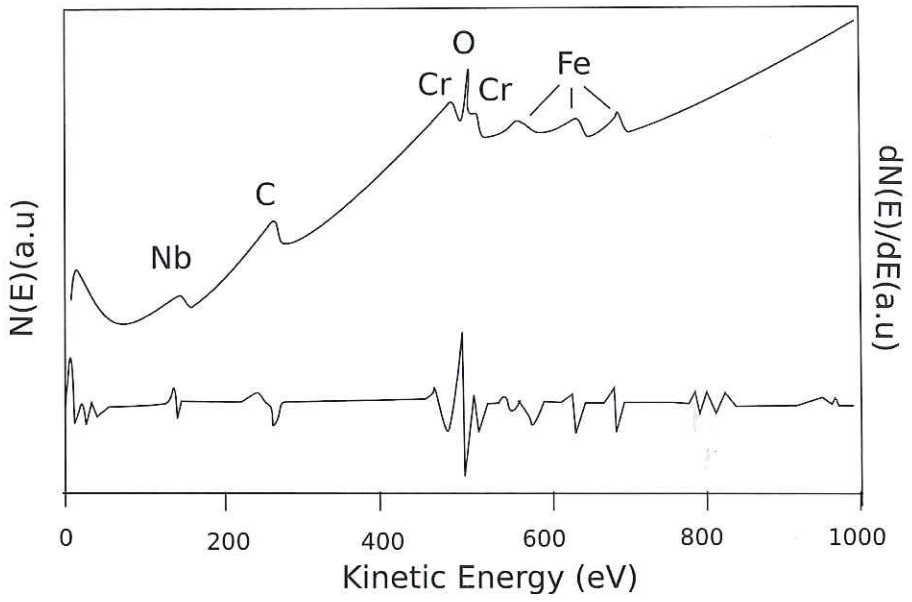

Figure 3.7 – Direct spectrum and differentiated spectrum of AES

3.4 X-ray reflectometry

The X - ray reflectivity (XRR) is an analytical tool, which can be used to measure thin film thickness, density and can also provide roughness information of surfaces and interfaces of thin films. Here we use it to measure the thin film thickness. The basic principle of XRR is that a grazing incident X - ray beam is reflected by the film surface and detected by a detector. By analysing the reflected intensity, the layer thicknesses can be determined.

A total external reflection occurs at the surface, when the grazing incident angle θ is smaller than critical angle θ_c. If θ is bigger than critical angle θ_c, the beam will be partly reflected and partly refracted as shown in Figure 3.8. The wave scattering can be described in the wave picture, as is shown in Figure 3.9. k_{in} is the wavevector of the incident wave and k_{out} is the wavevector of the scattered wave. The change in wavevectors (change in momentum) Q can be expressed as:

$$|Q| = 2|k_{in}| \sin\theta, \tag{3.8}$$

with $k = \frac{2\pi}{\lambda}$, we can obtain:

$$|Q| = \frac{4\pi \sin\theta}{\lambda}, \tag{3.9}$$

The reflected beam from the layer surface and from the interfaces will interfere with each other. There will be constructive interfereferences, when the phase shift equals an integer number n of the wave length λ. This condition is described by Bragg's law (Equation3.10) [13]. Here d_{hkl} is the interplanar spacing.

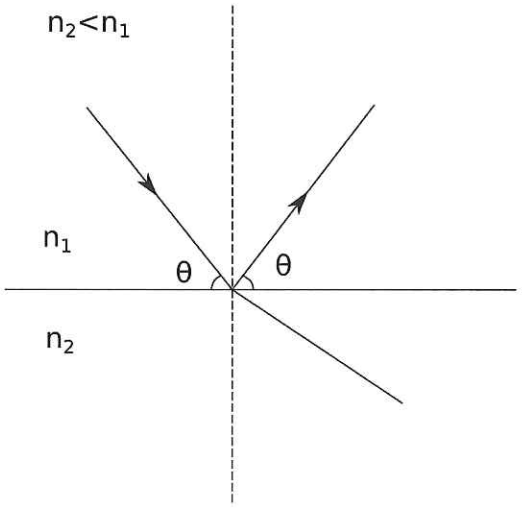

Figure 3.8 – Scattering of a x - ray beam with a incident angle θ at the interface of two layers with $n_2 < n_1$. The beam will be partly reflected and partly refracted.

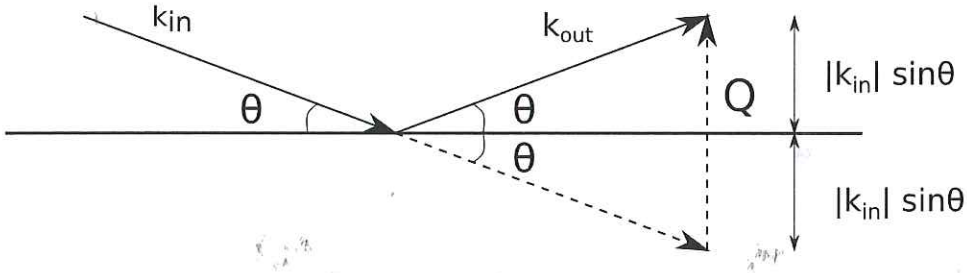

Figure 3.9 – This figure shows a wave scattering, where k_{in}, k_{out} are the wavevectors of the incident and the reflected beam. Here we assume it is an elastic scattering, so that $|k_{in}|$ equals $|k_{out}|$.

$$2d_{hkl} \sin\theta = n\lambda. \tag{3.10}$$

With combination of Equation 3.9 and Equation 3.10, we can obtain:

$$Q_n = \frac{2\pi n}{d_{hkl}}. \tag{3.11}$$

$$\Delta Q = Q_{n+1} - Q_n = \frac{2\pi}{d}. \tag{3.12}$$

The layer thickness $d = d_{hkl}$ can be determined from the oscillation curve of the reflected beams, as shown in Figure 3.10.

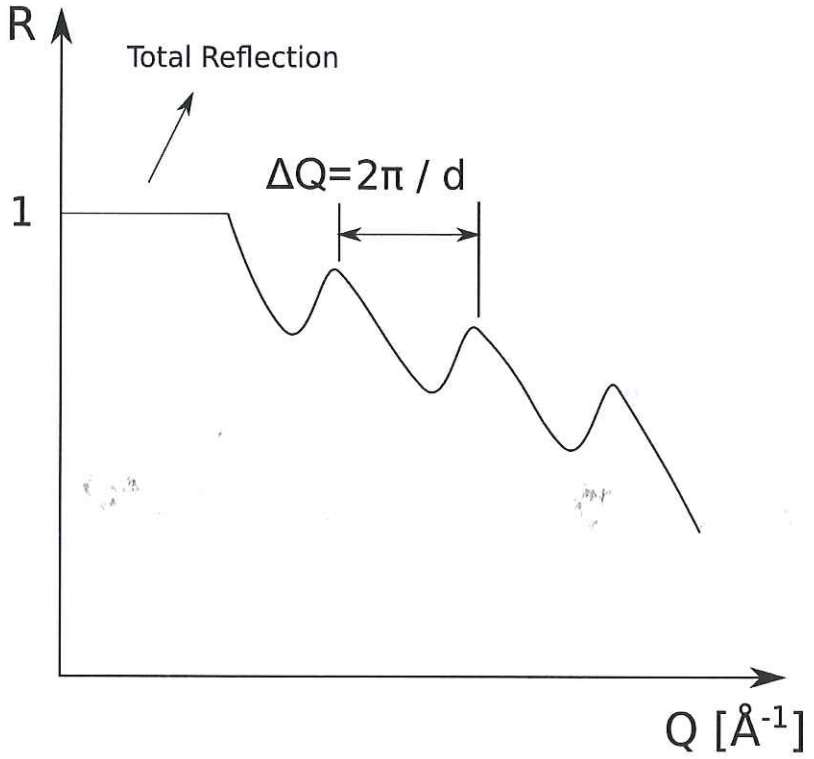

Figure 3.10 – This figure shows the oscillation curve due to interference of reflection from layer surface and interface of layer and substrate. Here the ordinate presents reflectivity. For the abscissa, the grazing incident angle θ is plotted in terms of Q and $Q = \frac{4\pi \sin\theta}{\lambda}$.

Chapter 4

Preliminary Works

In this Chapter, some preliminary works are introduced, such as preparing the filament, setting correct parameters for the sputter gun, optimizing the beam size, determination of sputtered position. First of all, the analysis chamber is introduced at the beginning to get a better understanding of the following work. Figure 4.1 is a schematic view of the analysis chamber. The sample is mounted on the manipulator, which can move in x_{M} and y_{M} directions. The sputter gun is not perpendicular to the sample and is about 45° tilted. It can control the beam in x_{G} and x_{G} directions. AES is mounted in the same chamber, so the sample can be analysed by it immediately after sputtering without transfer.

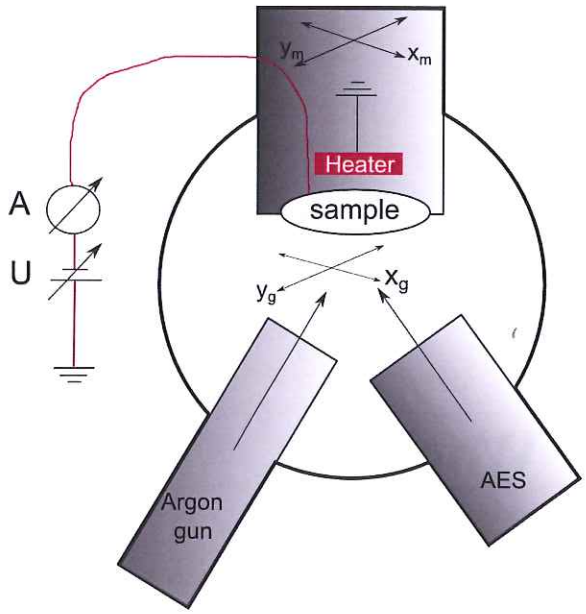

Figure 4.1 – Schematic of analyze chamber includes an Argon gun and AES.

4.1 Preparations of Sputter Gun

Before operating the sputter gun, some preparations are required, such as preparing the filament, degassing, setting proper parameters. Figure 4.2 shows the front panel of the source power supply. By pressing $0 \sim 9$ Keys, the display will show the corresponding parameters, the voltage, current,focus and so forth.

Figure 4.2 – Front view of PU-IQE 12/38

Firstly, the filament needs to be heated up slowly in "Stand by" mode. This procedure will sputter with ions from residual gas and also the gas desorbed from the walls [3]. Before normal operation the ion source also needs to be backed by using "Degas" function from the power supply. It is accessible after finish "Stand by" process. Before degassing, the pressure of ion source should be better than 10^{-6} mbar. After activing "Degas" mode, the emission current is increasing and the pressure of ion source will rise up to 10^{-3} mbar range and decrease after a few minutes. The "Degas" mode will last about 3 minutes and than change to "Standby" mode automatically. For the first time, the degassing process can be repeated for one or two more times. In this way, the lifetime of the filament is extended and it can decrease the contamination of ceramics in the ionizer and extractor assembly [3].

4.2 Start of Operation

To operate a sputter gun, the first step is to set appropriate parameters. Several user data have been stored in the machine. The parameter "Energy" defines the energy of ions. The parameter "Extractor " is used to set the voltage for extracting the ions from ionization assembly. "Focus 1" and "Focus 2" are responsible for focusing the beam. In a fine focused beam mode, they are around 80% [3]. In a high current mode, the "Focus 2" equals 0, so the beam has a large beam size. "Emission Current " is defined as the current emitted from the heated filament, this parameter is used to control the woking condition of filament.

After setting the parameters (or recalling one of the user data), the operation can

be started. By adjusting the pressure of the source, the sputter current can be controlled. In some range , there is a proportional relationship between source pressure, sputter current and energy current [3]. So the sputter current should be optimized through observing the changes on source pressure and energy current. Figure 4.3 shows the sputter current dependent on source pressure and Figure 4.4 shows dependent on energy current (user data #5). When the source pressure goes up to 10^{-3} mbar, I_{energy} starts to increase and the sputter current can be monitored by the ammeter. By adjusting the gas inlet valve slowly, the sputter current will get to a maximum. The value of sputter current is always slightly different for every operation, even the pressure of source and energy current are totally the same with before. During the operation the first pumping stage should be closed. It only opens, when preparing the filament or degassing the sputter gun.

As mentioned before, there are two different operation modes. For a fine focused beam, the maximum sputter current can go up to 0.4 μA. For a high current mode, the maximum sputter current is around 1.7 μA. For the all of experiments here, we use the sputter gun with the user data #5. The working conditions of the gun are listed in Table 4.1.

Table 4.1 – Working conditions for user data #5

Source Pressure	7.4×10^{-3} mbar
Energy Current	62 μA
Sputter Current	0.40 μA

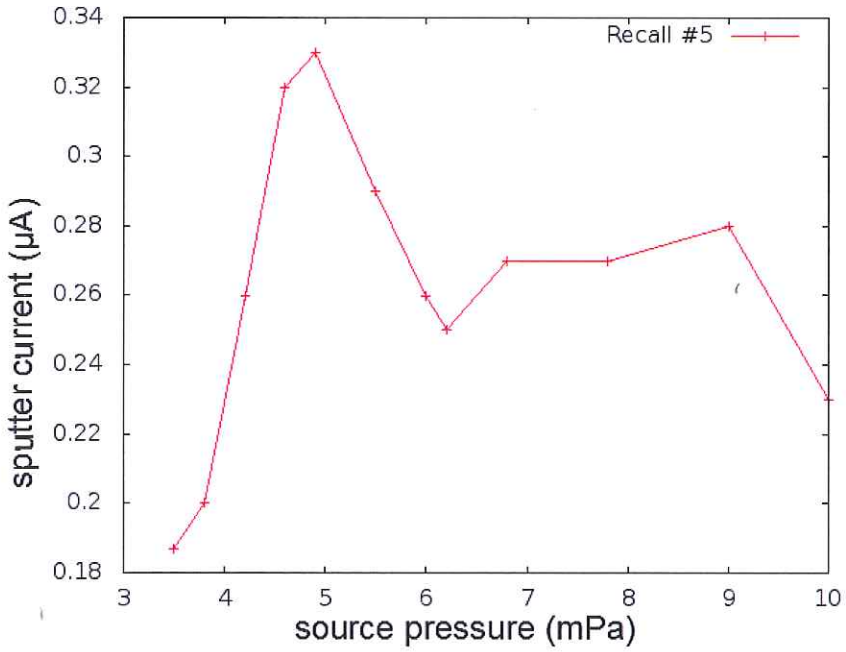

Figure 4.3 – Sputter current increases by increasing source pressure and get to a maximum. Then it starts to decrease to some point and stays nearly stable at the end.

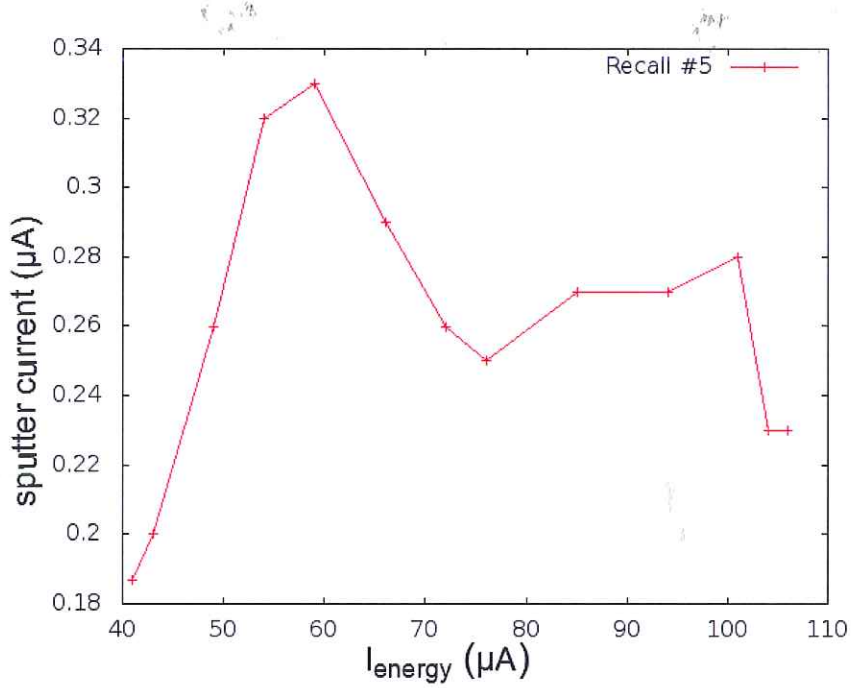

Figure 4.4 – Sputter current change dependent on energy current is almost the same with the change dependent on source pressure.

4.3 Optimization of Beam Size

The beam is focused by two focus lenses in the source IQE 12/38. Since stored settings are used, it is already optimized for a focused beam. Next step is to change the distance between the gun and sample, so that the focus of the beam is on the sample surface. As shown in Figure 4.5, a label is mounted on the linear transfer flange to mark the distance. Here 6 positions are chosen. The different positions on the label are numbered as shown in the Figure 4.6.

Figure 4.5 – The left side of the picture shows a part of the deflection section of the sputter gun. The label is mounted on a linear transfer flange, which can adjust the distance between sputter gun and sample.

A sample with a pinhole is used to determined the beam size on the sample. The size of the pinhole (d=1.5 mm) is larger than the beam size (0.2 μm $\sim$ 0.3 μm), which means that the beam can totally pass through the pinhole. When the beam

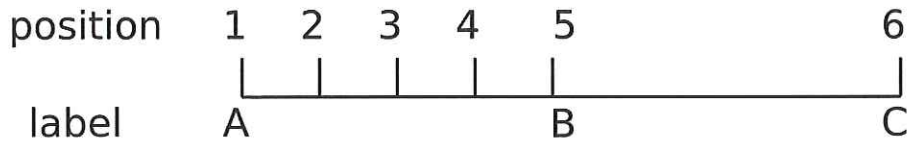

Figure 4.6 – Each number represents a position on the label. In other words, each number represents a distance between sputter gun and sample. The distance between A and B is equally divided by position 2, 3, 4.

goes through the pinhole, all the ions hit the heater behind the sample and go to ground without passing the ammeter. Consequently the ammeter shows a current around 0 A. When moving the sample with the pinhole across the beam, the current changes dependent on the position of the beam relative to the pinhole. Thus, the profile of the beam is recorded.

The intensity distribution of the ion beam can be regarded as a Gaussian function (Equation 4.1).

$$f(x, \mu, \delta) = \frac{1}{\delta\sqrt{2\pi}} e^{-\frac{(x-\mu)^2}{2\delta^2}}, \tag{4.1}$$

with

μ	expectation value,
δ	standard deviation.

The pinhole can be regarded as step functions. When the beam pass across the pinhole, the current represents the convolution of a Gaussian function and step functions (please see Figure 4.7).

The flange of sputter gun was put to the position 1 and the sample was moved via the manipulator to find the pinhole. The position of pinhole on the manipulator is around x_{M}=5.4 mm, y_{M}=18.5 mm. To determine the profile of the beam, the manipulator was moved in one direction, so the sample was fixed in y direction

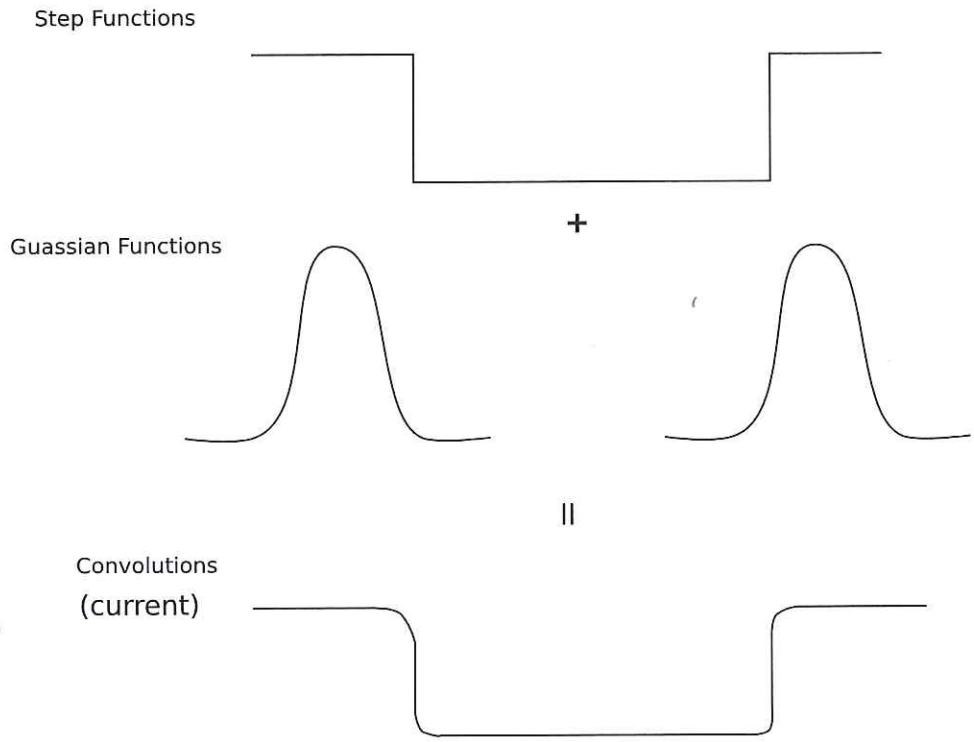

Figure 4.7 – The recorded current represents the convolution of pinhole with beam profile.

(y_M=18.5 mm) and was moved only in x direction (x_M=1.4 $\sim$ 3.5 mm). When the sample was moved step by step across the pinhole, the currents showed on ammeter were recorded. The current decreased and went to a minimum, when the beam went through the pinhole. After moving the sample for some distance, the current increased, since the beam was getting out from the pinhole. With the current changes, the middle of the pinhole position can be determined relatively exactly. If the pinhole's y - value has a big difference with the first fixed y - value, the measurement needs to be repeated again, because the beam may not go across the center of pinhole and the complete profile of the beam can not be shown. Fix the manipulator's x - value and do the same measurements, which move the sample only in y direction. In this way, the profile of the beam can be determined. The same measurements for the other 5 positions were done in the same way.

The Figure 4.8 shows the curve of current change fitted by Gaussian curves. From the fitting results, the standard deviation δ can be obtained. If we take the δ to the Equation 4.2, the FWHM of the beam can be calculated.

$$\text{FWHM} = 2\sqrt{2ln2}\,\delta = 2.355\,\delta \tag{4.2}$$

The beamsize for different positions are shown in Figure 4.9. The abscissa represents the sample's position on the manipulator and the ordinate is the beam size. From the results, we can see that position 2 is the ideal position. The minimum beam size is about 190 μm.

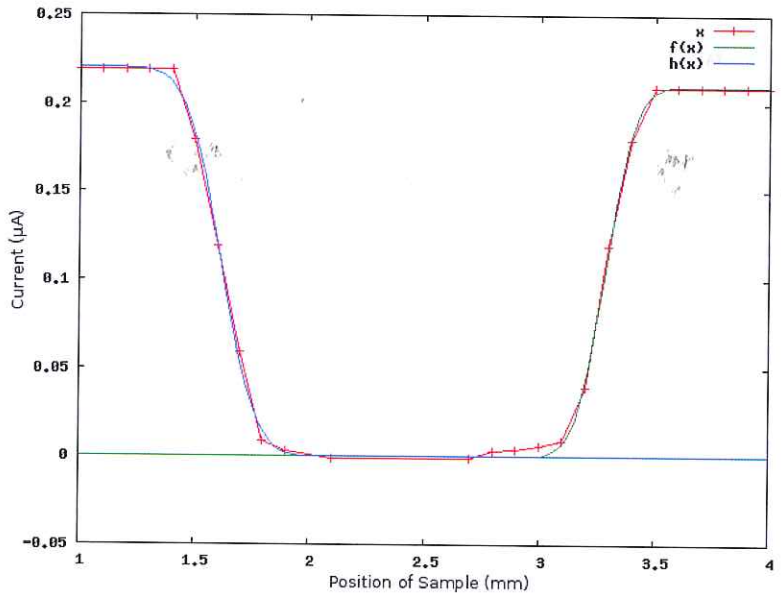

Figure 4.8 – The abscissa represents the position of the sample on the manipulator, which adjusted by manipulator, and the ordinate is the recorded current. This figure shows the current changes, when the sample was moved in x - direction at position 1. f(x) and h(x) are the fitted Gaussian curves.

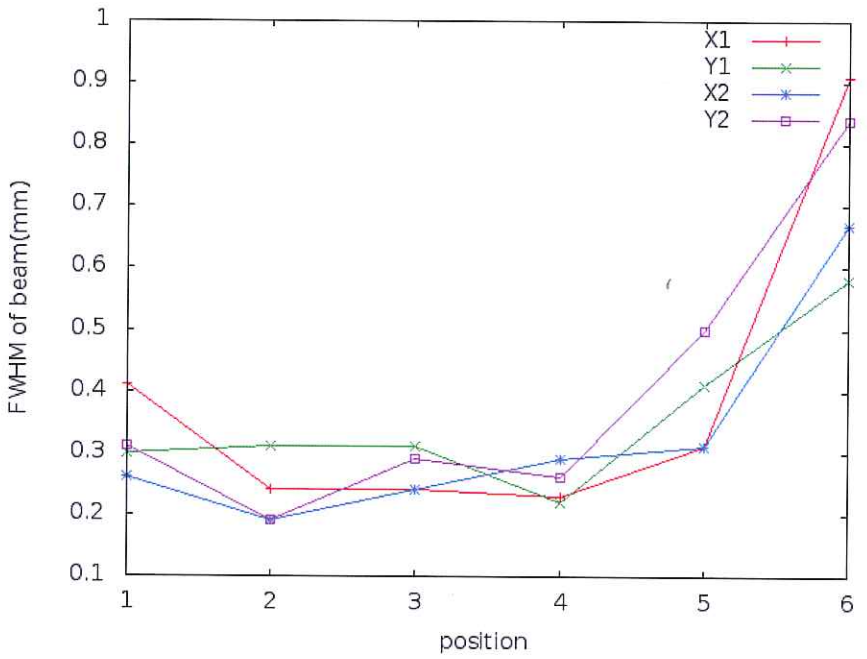

Figure 4.9 – This figure shows the beam size changes for different distances between sample and sputter gun. x_1, x_2 represent the results from the measurements, which beam went across pinhole in x - direction.

4.4 Sputter Position

The sputter position can be chosen in three different ways: moving the beam, moving the sample or combine these two. The beam can be moved easily by using the source power supply. The parameters 'Position x' and 'Position y' define the middle of the scanned area. The scanned width can be adjusted by changing the parameter 'Width x ' and 'Width y ' . The range spans from -5 mm to 5 mm, which means that maximum sputter square is 10 mm$\times$10 mm centered at zero position.

The another way to choose sputter position is moving the sample. The sample can be moved by the manipulator in x_{M} and y_{M} directions, which is not consistent with beam's moving directions x_{G} and y_{G}. A matrix is required, which can transform the positions between the two coordinates systems, so that the sputter

position can be calculated. There is an angle between the two coordinates and also an offset between the origins of two coordinates. Since there is a distance between the sputter gun and sample, the sputtered patterns are slightly enlarged. These three matrix need to be considered.

$$\text{Offset} = \begin{pmatrix} d_x \\ d_y \end{pmatrix}, \tag{4.3}$$

$$\text{Rotation} = \begin{pmatrix} \cos\alpha & -\sin\alpha \\ \sin\alpha & \cos\alpha \end{pmatrix}, \tag{4.4}$$

$$\text{Scale} = \begin{pmatrix} s & 0 \\ 0 & s \end{pmatrix}. \tag{4.5}$$

The required matrix is the combination of these three matrix as follow :

$$\begin{pmatrix} x_{\mathrm{M}} \\ y_{\mathrm{M}} \end{pmatrix} = \begin{pmatrix} d_x \\ d_y \end{pmatrix} + \begin{pmatrix} \cos\alpha & -\sin\alpha \\ \sin\alpha & \cos\alpha \end{pmatrix} \begin{pmatrix} s & 0 \\ 0 & s \end{pmatrix} \begin{pmatrix} x_{\mathrm{G}} \\ y_{\mathrm{G}} \end{pmatrix}$$

To calculate the matrix, three measurements were done. For the first, the sputter gun was set to zero position and the sample was moved by manipulator to let the beam pass through the pinhole. The pinhole's position x_{M}=5.4 mm, y_{M}=18.5 mm correspond the offset d_x, d_y. For the second, the sample was fix at position x_{M}=7.4 mm, y_{M}=15.4 mm and the beam was moved to find the pinhole. When the beam passed through the pinhole, the beam's position was x_{G}=1.6 mm, y_{G}=-2.8 mm. For the third, the beam was fixed at x_{G}=-2 mm, y_{G}=1 mm

and the sample was at position x_M=3.13 mm, y_M=19.3 mm, when the beam went through the pinhole. With these three measurements, the matrix can be calculated and the result is shown in Equation 4.6. With this matrix, the the sputter position on the sample can be calculated.

$$\begin{pmatrix} x_M \\ y_M \end{pmatrix} = \begin{pmatrix} 5.4 \\ 18.5 \end{pmatrix} + \begin{pmatrix} 1.106 & -0.057 \\ 0.057 & 1.106 \end{pmatrix} \begin{pmatrix} x_G \\ y_G \end{pmatrix} \tag{4.6}$$

With the invert matrix 4.7, the position on the sample can be transformed to position of the beam.

$$\begin{pmatrix} x_G \\ y_G \end{pmatrix} = \begin{pmatrix} -5.8 \\ -16.3 \end{pmatrix} + \begin{pmatrix} 0.9 & 0.05 \\ -0.05 & 0.9 \end{pmatrix} \begin{pmatrix} x_M \\ y_M \end{pmatrix} \tag{4.7}$$

For an example, a dot expected to be sputtered at the position, which need to move sample 1 mm in x_M - direction and 1.5 mm in y_M - direction. In this case, the dot can be sputtered at exact position by moving the beam in x_G - direction for 0.9 mm, for x_G - direction for 1.35 mm instead of moving the sample.
With these two matrix, the sputter position can be known. When the sputter position is known , it is also possible for AES to find it quickly.

Sample Orientation

The manipulator can not only move the sample in two directions, but also rotate it. To sputter at a expected position on the sample, only knowing the sputter position is not enough. The sample should also be right orientated. The rotation of

the sample and the center position of the sample need to be determined. There is a rotator on the manipulator. When it turns two rounds, the sample will turn one. There are some marks on the rotator as shown in Figure 4.10, which can indicate the rotation angle. Before the sample is loaded on the manipulator, the sample should be put in the trolly as showed in Figure 4.11. The 'ear' of the sample holder, which is perpendicular to the sample edge, is put on the right side. In this way, the sample's orientation is always the same, when it is loaded on the manipulator.

Here we expect that after rotating the sample the sample's edges will be parallel or perpendicular to the coordinate of sputter gun. Several lines (Width x=0 mm, Width y=8 mm) were sputtered, which can indicate the y direction of the sputter gun. After sputtering a line, the sample was rotated a little bit and sputtered with another line. Figure 4.12 shows several sputtered lines. When the sample was taken out of the chamber, the lines were checked by eyes. The line, which is most accurately parallel or perpendicular to the edges, was picked out. This position is taken as a reference. Here at 190° (read from the marks), the y axis of sputter gun is perpendicular or parallel to the edges of the sample. The next step is to determine the center of the sample. Using the similar method, some dots were sputtered on the sample. Firstly, the sample was rotated to position 190° and the beam was set to zero position (x_G=0, y_G=0). Several sputter positions were chosen by moving the sample. After the sputtering, the dots were checked by eyes and the most centered one was chosen. The sputtered lines and dots are shown in Figure 4.13. x_M=5.4 mm, y_M=18.5 mm is the position, which sputter gun's zero position hits the center of the sample.

With these experiments we can known that, when the sample is rotated to 190° ,

the sample's edges will be parallel or perpendicular to the sputter gun's coordinate. The zero position of sputter gun will hits the sample center, when the sample is moved to x_{M}=5.4 mm, y_{M}=18.5 mm on the manipulator.

Figure 4.10 – The paper with marks is stuck on the center of the rotator, which does not rotate during rotation. A small rod is fixed at the outer shell, which can be rotated with the rotator. With the indicated degrees, the rotation angle can be known.

Figure 4.11 – The sample should be put on the trolly in this orientation for every sputtering. The 'ear' of the sample holder, which is perpendicular to the sample edge, is put on the right side.

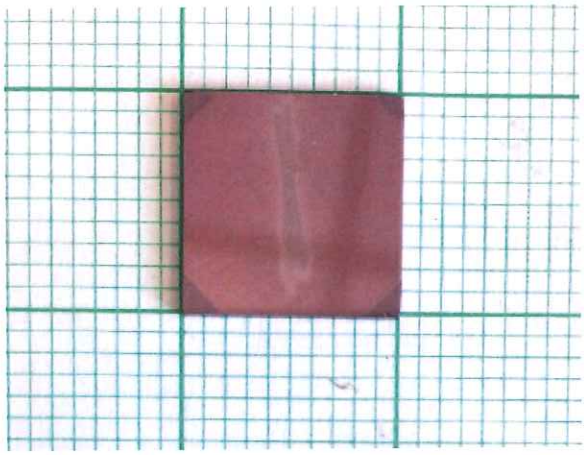

Figure 4.12 – Several lines were sputtered to determine the orientation of the sample.

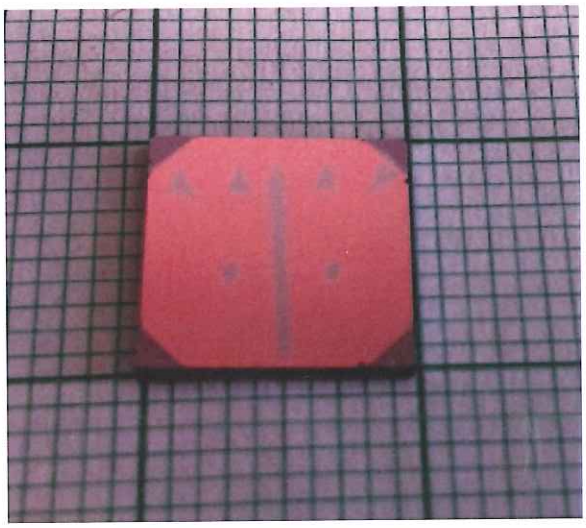

Figure 4.13 – The line was sputtered to know whether the sample is right orientated. The dots are used to check the center of the sample.

Chapter 5

Results and Discussion

Determination of sputter rate for different materials is the most important step. Since the sputter rate is a key parameter for depth profiling. In this chapter, the method of calculating sputter rate and the results will be discussed. In order to determine the sputter rate, a thin layer is grown on the sample by MBE. Then, the sample is transferred to analysis chamber and analysed by AES after each sputtering process. With the AES spectrum the thickness of layer can be calculated. For a accurate thickness measurement, the samples are sent to XRR. With the thickness change and sputter time, the sputter rate can be calculated.

5.1 Measurement 1

For the first sample, Si was selected as the substrate and coated with 5 nm Au on the surface. 7 small squares (1 mm$\times$1 mm) were sputtered on the sample and each square was sputtered for different long time, as shown in table 5.1. The sputtered sample is shown in Figure 5.1. After each sputtering the sample was

analysed by AES and got a spectrum. Figure 5.2 shows the intensity changes according to sputtering time.

After sputtering, the sample was sent to XRR, but because of the roughness, it was impossible to get the thickness information. As shown in figure 5.2, the intensity of Au dose not decrease exponentially by sputtering time and it dose not change much at the end. The diagram indicates that the intensity will not go to 0 even though the noise from the background has been taken into account.

Table 5.1 – Sputter time for different positions

Square	1	2	3	4	5	6	7
Sputtering time/s	30	40	50	70	90	110	120

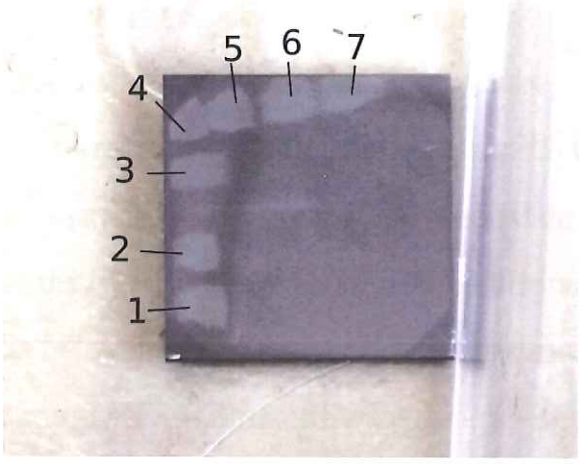

Figure 5.1 – 7 squares were sputtered along the edge. Then the edges were cut off and the rest of sample was sent to XRR for a thickness measurement

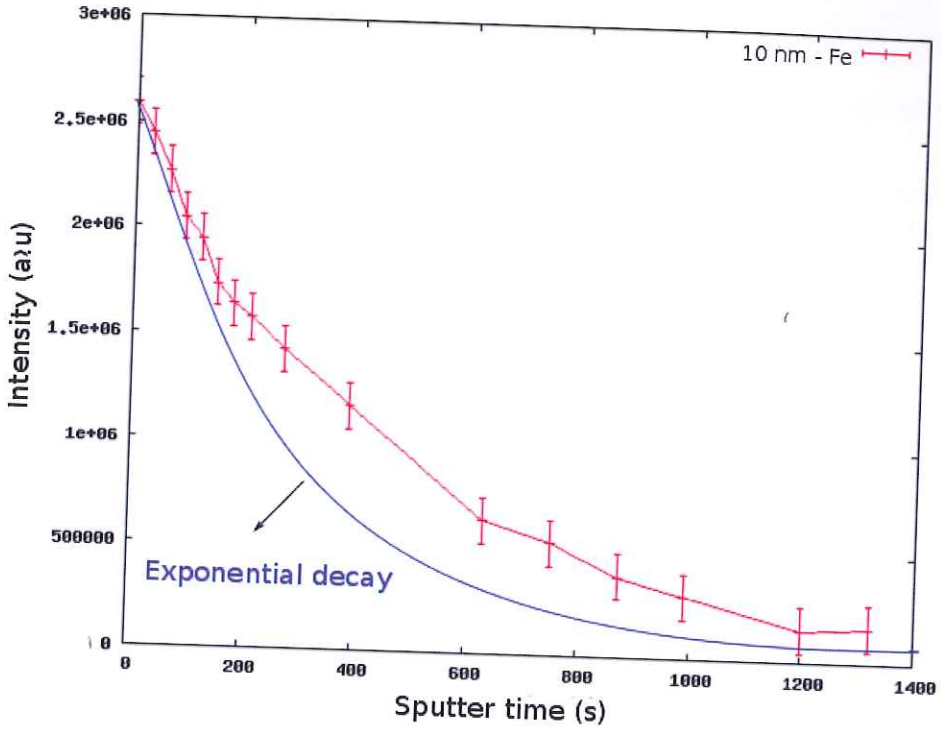

Figure 5.2 – Intensity of Au measured by AES decreases by increasing sputter time. At the end the intensity does not change much but still much bigger than 0.

5.2 Measurement 2

This time we did the sputtering and thickness measurement on two different samples, one was used for sputtering and another was for XRR measurement. A 4 - samples sample holder is used here. Two GaAs substrates were put in the sample holder and the other two places were filled with two blocks. As shown in Figure 5.3, the two substrates on right sides are GaAs substrates. In this way, all the substrates can be deposited with same thick layers. Sputter on one of the substrate and send the other to XRR, so that initial thickness can be checked. For the deposited material, this time we chose Fe, since Au has a relatively small peak height on the AES spectrum. After sputtering the hight of Au - peak will get smaller and will be hard to recognize. Fe has a bigger peak - hight than

Au, so the samples were deposited with 10 nm Fe. A 2 mm $\times$ 2 mm square was sputtered for 22 minutes step by step.

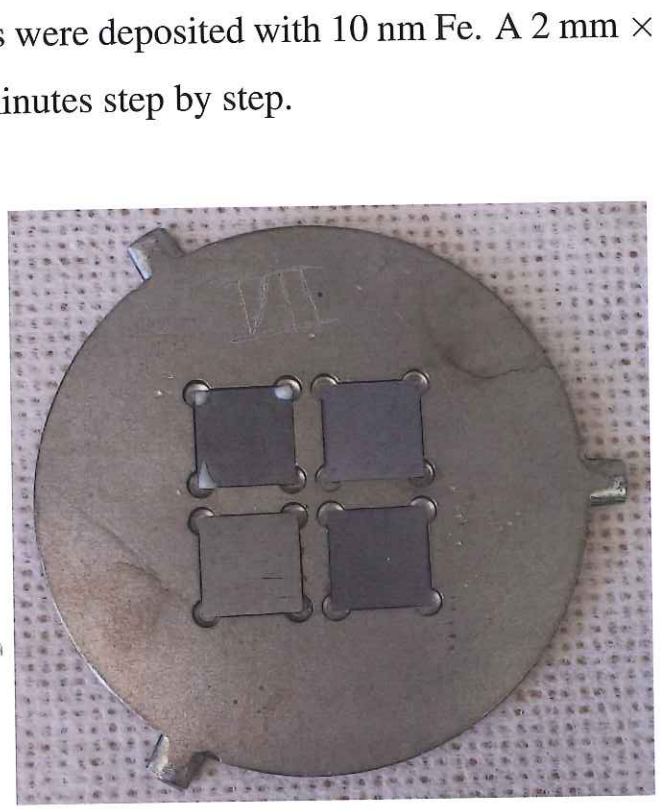

Figure 5.3 – The samples on the right side are the GaAs substrates.

The result is shown in Figure 5.5. The intensity decreases not exactly exponentially. With the spectrum of AES, the layer thickness can be calculated. The intensity of layer material attenuates exponentially by decreasing of layer thickness [14]. The relationship between intensity and layer thickness is shown by Equation 5.1. Here the Equation 5.1 is transformed to Equation 5.2, which demonstrates the relationship between $\frac{I}{I_0}$ (ratio of the intensity to the initial intensity) measured by AES and thickness of Fe layer. Figure 5.4 shows the thickness of Fe layer dependent on $\frac{I}{I_0}$. From the Figure 5.4, it can be observed that when the layer gets thicker, the intensity ratio flattens out around 1. It means that, when the layer is thick, a small error in $\frac{I}{I_0}$ will result in huge error of calculated thickness. The error of calculated thickness will get bigger, when the layer is thicker. For a thick layer, the AES is not recommended for measuring

the thickness, since error is huge. The thickness z is a function of two variables I_0 and I. The error of thickness Δz can be calculated by Equation 5.3. ΔI_0 is the uncertainty of I_0 and ΔI the uncertainty of I. Here both uncertainties are due to the noise of AES.

$$I = I_0(1 - e^{-\frac{-z}{\lambda(E_0)}} e^{-\frac{-z}{\lambda(E_1)}}), \tag{5.1}$$

$$z = \frac{-\ln(1 - \frac{I}{I_0})}{0.1034}, \tag{5.2}$$

with

z	layer thickness,
I	Intensity of layer material of thickness z,
I_0	Intensity of layer material before sputtering ,
$\lambda(E_0)$	the inelastic mean free path for the incident electron with energy E_0,
$\lambda(E_1)$	the inelastic mean free path for the ejected electron with energy E_1.

$$z = z(I_0, I),$$

$$\Delta z = \sqrt{\left(\frac{\partial z}{\partial I_0}\right)^2 {\Delta I_0}^2 + \left(\frac{\partial z}{\partial I}\right)^2 \Delta I^2}, \tag{5.3}$$

with

ΔI_0	uncertainty of I_0,
ΔI	uncertainty of ΔI,

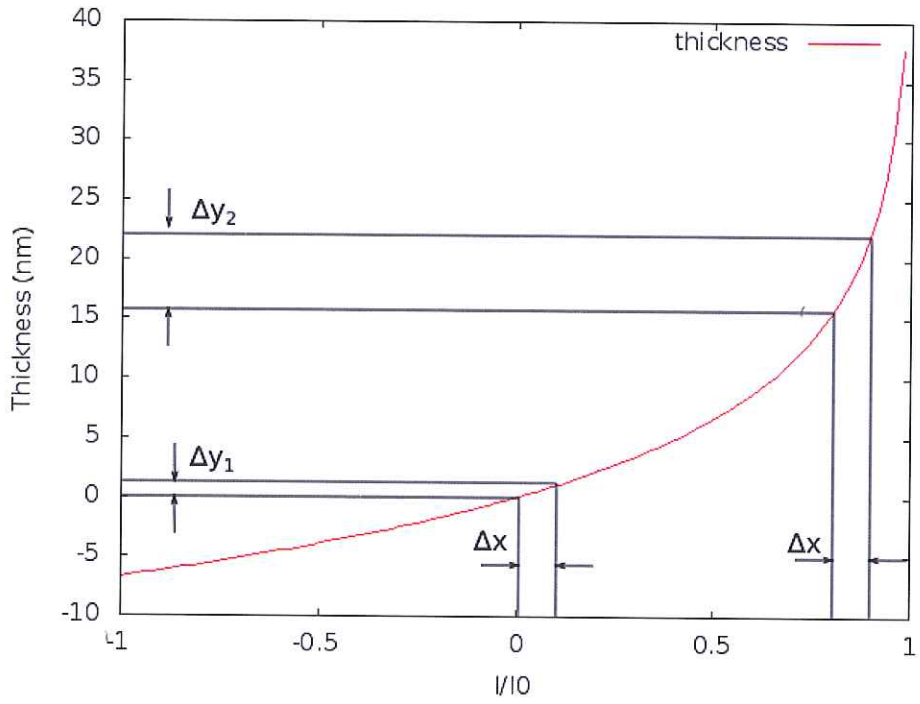

Figure 5.4 – This figure shows calculated thickness of Fe layer dependent on intensity ratio. For the same uncertainty Δx in intensity ratio, the thicker layer has a bigger error Δy_2 in calculated thickness than the error Δy_1 for a thinner layer.

In Figure 5.6 the intensity is transformed to thickness. We can see that there is no linear dependency between the layer thickness and the sputter time. At the end the intensity of Fe is not at 0, but it does not change anymore. The result is very similar to the first measurement. This could happen because of the error of AES. We can see the error from AES is huge. Another explanation for this phenomenon is that there is atomic mixing at the interface of the layer and substrate. For the next measurement, The sample needs to be sent to XRR for a 'real' thickness measurement. In this way, we can measure the 'real' thickness (not by calculation) and know whether the phenomenon is caused by error of AES.

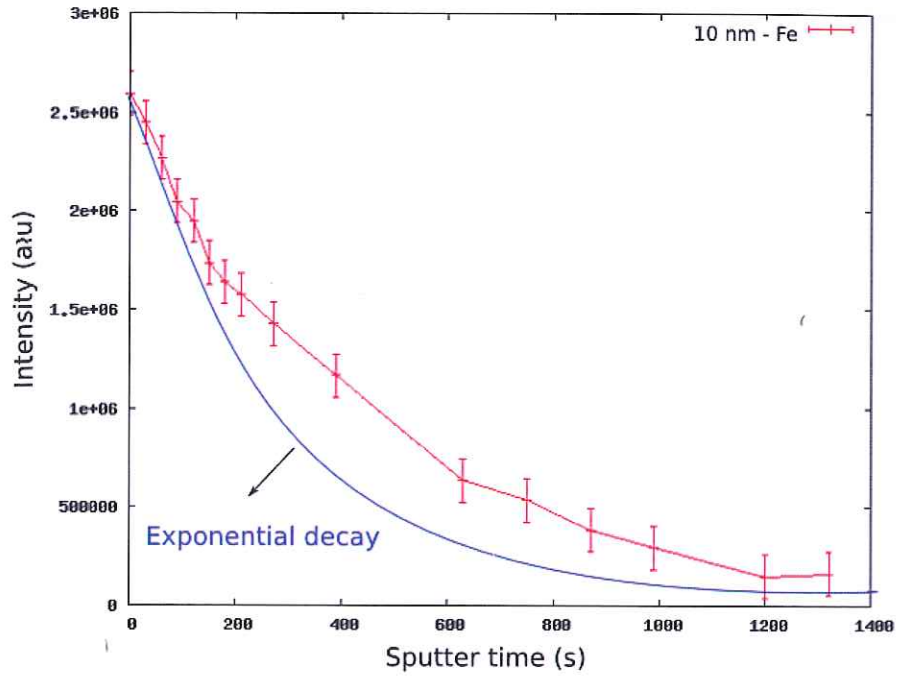

Figure 5.5 – Intensity of Fe (measured by AES) not exponentially dependent on sputter time

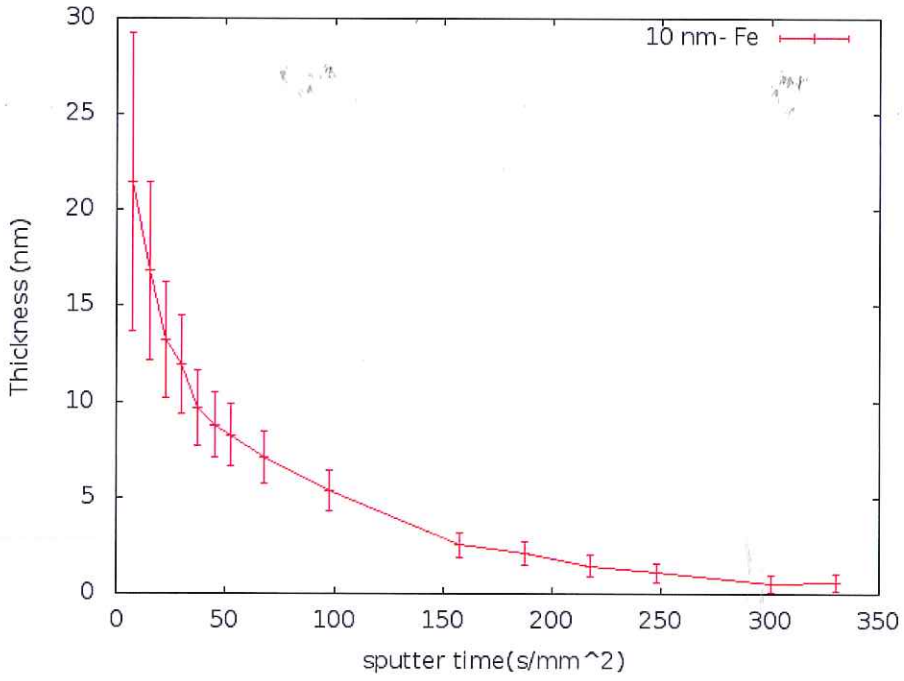

Figure 5.6 – Calculated thickness of Fe versus sputter time. There is no linear dependency between layer thickness and sputter time.

5.3 Measurement 3

To check the assumptions, the third measurement was prepared. For this measurement, 4 Si substrates were put into one sample holder to get equally thick layers. The layer was again 10 nm Fe. They were sent to XRR for thickness measurement after sputtering. With XRR, it is difficult to let the x - ray incident on the exact sputtered position, especially when the sputtered area is small, so here the whole sample surfaces were sputtered (10 mm $\times$ 10 mm).

The sputter time for these 4 samples were chosen from 4 measurement points from the last sample, which indicate the change of sputter rate. The chosen measurement points were 40s, 90s, 180s and 270s as shown in Figure 5.7. From the first and second measurement points, we can see that there is linear dependency between thickness and sputter time. But from third and fourth, we can see the thickness does not decrease linearly any more. For this measurement, we try to sputter the same depth as these four measurement points. It is possible, when we get the same sputter conditions. With the measurements by XRR, we could know the 'real' layer thickness at these four points and could compare them with the results calculated by AES. Since the sputtered area of this measurement is bigger than last one by 8 times, the corresponding sputter time should be enlarged by 8 times as well. Thus, for these 4 samples, the sputter times were 16min, 40min, 80min and 110min. After sputtering, the individual samples of layers were measured by XRR. The results are shown in Table 5.2.

Figure 5.8 shows the sputtered depth dependent on sputter time. We can see that the three lines shows similar shapes. Even the thickness was measured by XRR, the sputtered thickness is still not linearly dependent on sputter time. We can come to a conclusion that the result is not due to the error from AES. It should

result from atomic mixing at the interface of layer and substrate.

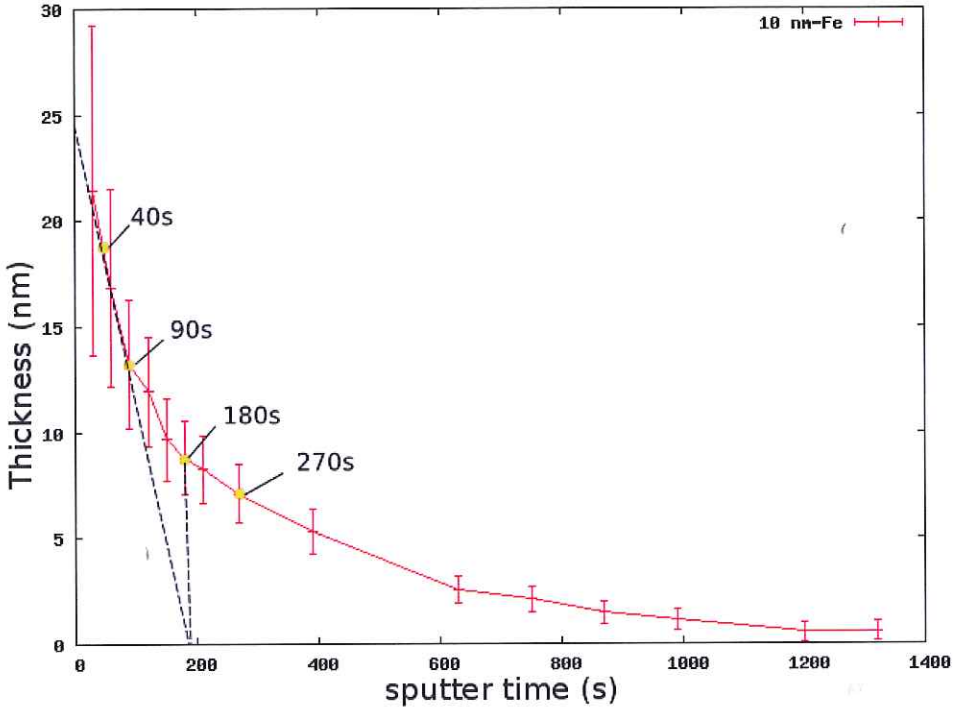

Figure 5.7 – 4 measurements points are chosen from the second measurement

Table 5.2 – Thickness measured by XRR

Sample	1	2	3	4
Sputter time (min)	16	40	80	110
Fe (nm)	62.5	70	85	110
Error (nm)	±1	±3	±2	±2

The atomic mixing during sputtering has been proved in many papers [15][16][17] . Here the atomic mixing is a process, that two different atomic species mix across the interface because of ion beam sputtering. The energy of the ion beam is 5 keV, so it belongs to low energy ion beam mixing. The atomic mixing can be explained by ion/solid interaction. When an ion beam incident on the sample surface, there occurs collisions. When the surface atom is hit by an incident ion,

the energy and momentum may be transferred from an ion to a surface atom. If the transferred energy is big enough to overcome the surface binding energy, the atom may be ejected from the sample, which means the atom is sputtered off. An other possibility is that the accelerated atom may hit another one and so forth and results in a displacement cascade [17]. The multiple displacements of atoms result in atomic mixing across the interface of the layer and the substrate. Each incident ion results in a small volume containing layer atoms and substrate atoms. These cascades will overlap by increasing ions and form a mixing region. This atomic mixing process happens in a few picoseconds [17]. The mixing depth W remains stable during the sputtering and the mixing depth is related to ion energies [16]. The experiment done by D.W. Hoffman [15] and Z. L. Liau [16] shows that for 2 keV Ar^+, the mixing thickness is around 3 nm; for 7 keV Ar^+, the mixing depth is 8.7 nm; for 10 keV Xe^+, the mixing depth is 10 nm. There is nearly linear dependency between mixing depth and ion energy. In our case, the ion energy is 5 keV, the mixing depth should around $6 \sim 7$ nm. When the Ar ions approach the mixing region, they sputter not only the Fe layer, but also Si substrate [16]. This can explain the phenomena that layer thickness does not decrease linearly.

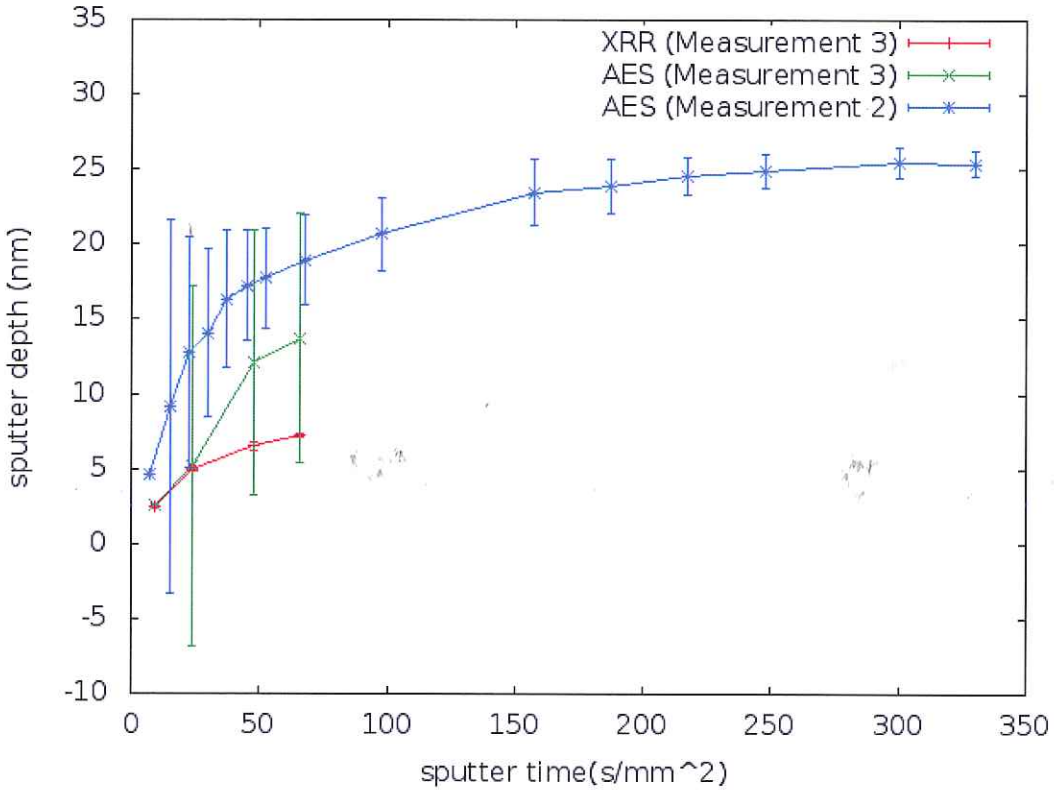

Figure 5.8 – Thickness of Fe determined by AES and XRR for measurement 2 and3 versus sputter time

Chapter 6

Conclusion and Outlook

6.1 Conclusion

For the sputter rate determination, three measurements have been done. For the first measurement, 5 nm Au is deposited on Si substrate; for second, 10 nm Fe is deposited on GaAs substrates and the last measurement, 10 nm Fe is coated on Si. The first two measurements all show that the sputter rate decreases by increasing sputtered depth and the intensity of layer does not tend to 0 after a long - time sputtering. For the third measurement, the substrate is coated with 10 nm Fe and sputter in the same way as the second measurement, but this time the sputtered samples are sent to XRR to get a 'real' thickness measurement. For the third measurement, the result is still the same with the first two. This means the result is not due to the error of AES, but because of the atomic mixing across the interface of layer and substrate. In our case, we used 5 keV Ar^+ to sputter 10 nm iron layer. The mixing depth is estimated as $6 \sim 7$ nm. This is the reason why we can find that sputtered depth decreases linearly by increasing sputter time at the beginning then decreases slower and slower.

6.2 Outlook

For further determinations of sputter rate, the layer should be thick enough. The energy of sputter ion is 5 keV and the corresponding mixing depth is around 7 nm, so the layer should be much thicker than mixing depth, for example 50 nm. Another way to reduce the influence of atomic mixing is using lower ion energies to sputter. Since the mixing depth is nearly proportional to the ion energies, lower ion energies are accompanied by a thinner mixing depth. In this way, there should be a linear dependency between thickness and sputter time during the most of sputter process and the calculation of sputter rate will be much more accurate. The thickness of the layer should be measured by XRR instead of AES, since the error from AES gets bigger for a thicker layer. When do the measurement, the samples should be transferred as soon as possible to decrease the oxidation.

Bibliography

[1] Garima Agarwal I.P. Jain. Ion beam induced surface and interface engineering. *Surface Science Reports 66*, 66(3-4):95–96, 3 2011.

[2] Cedric John Powell Alvin W. Czanderna, Theodore E. Madey. *Beam Effects, Surface Topography, and Depth Profiling in Surface Analysis*, chapter The Technology and Design of Molecular Beam Exitaxy Systems, pages 118–119. Springer Science Business Media, 1998.

[3] SPECS Surface Nano Analysis GmbH, Voltastrasse5, 13355 Berlin, Germany. *SPECS User Manual, PU IQE 12/38-Ion Source Power Supply*, 3 edition, 4 2013.

[4] Introduction to electron and ion guns. website. `www.kimphys.com/electron_guns/catalog_PDFs/Gun_intro_prelim.pdf`.

[5] SPECS Surface Nano Analysis GmbH, Voltastrasse5, 13355 Berlin, Germany. *SPECS User Manual, Wien Mass Filter for SPECS IQE 12/38 WF-IQE including Wien Filter Power Supply PS-WF*, 3 edition, 4 2013. Basic Principle Of Operation.

[6] Alexandaer Weber. Preparation of functional oxide multilayers. Technical report, Forschungszentrum Juelich, Februray 2014.

[7] Jens Reichow. Instruction book. DCA MBE M600 Molecular Beam Epitaxy System, Technical System Description, Chapter 2. System Layout, Page 7.

[8] Robin F.C. Farrow. *Molecular Beam Epitaxy: Applications to Key Materials*, chapter 1.The Technology and Design of Molecular Beam Exitaxy Systems, page 24. Elsevier, 1995.

[9] G. Biasiol and L. Sorba. Molecular beam epitaxy: Principles and applications. *Crystal growth of materials for energy production and energy-saving applications*, page 68, 2001.

[10] Krishna Seshan. *Handbook of Thin Film Deposition*, chapter 10.Molecular Beam Epitaxy:Equipment and Practice, page 408. William Andrew, 2011.

[11] H. Lüth. *Solid Surfaces, Interfaces and Thin Films*. Graduate Texts in Physics. Springer-Verlag, 2010. Auger Electon Spectroscopy (AES).

[12] Auger electron. website. `fys.kuleuven.be/iks/nvsf/experimental-facilities/surface-analysis-chamber`.

[13] R. Serway and J. Jewett. *Physics for Scientists and Engineers, Volume 2, Chapters 23-46*. Cengage Learning, 2010. Wave Optics.

[14] A. Jablonski and J. Zemek. Overlayer thickness determination by xps using the multiline approach. *Surface and Interface Analysis*, 46(9):193–204, 9 2014.

[15] J.R. MONKOWSKI I.S.T. TSONG and D.W. HOFFMAN. Ion-beam-induced atomic mixing at the sio2/si interface. *Nuclear Instruments and Methods*, 182/183:237–240, 1981.

[16] B.Y.Tsaur Z.L.Liau and J.W.Mayer. Influence o f atomic mixing and preferential sputtering ondepth profiles and interfaces. *J. Vac. Sci. Technol.*, 16:121–127, 1979.

[17] Garima Agarwal I.P. Jain. Ion beam induced surface and interface engineering. *Surface Science Reports 66*, pages 95–96, 2011.